Available online at www.sciencedirect.com
ScienceDirect
Intermetallics 15 (2007) 583–592
Intermetallics
www.elsevier.com/locate/intermet

Complex magnetic properties of $Ho_3Cu_4Sn_4$

Ł. Gondek [a,*], A. Szytuła [b], D. Kaczorowski [c], A. Szewczyk [d], M. Gutowska [d], O. Prokhnenko [e]

[a] Faculty of Physics and Applied Computer Science, AGH University of Science and Technology, Mickiewicza 30, 30-059 Kraków, Poland
[b] M. Smoluchowski Institute of Physics, Jagiellonian University, Reymonta 4, 30-059 Kraków, Poland
[c] W. Trzebiatowski Institute of Low Temperature and Structure Research, Polish Academy of Sciences, P.O. Box 1410, 50-950 Wrocław, Poland
[d] Institute of Physics, Polish Academy of Sciences, Lotników 32/46, 02-668 Warszawa, Poland
[e] Berlin Neutron Scattering Center, Hahn-Meitner Institute, Glienicker Strasse 100, D-14 109 Berlin, Germany

Received 7 March 2006; received in revised form 30 June 2006; accepted 4 October 2006
Available online 27 November 2006

Abstract

The $Ho_3Cu_4Sn_4$ compound exhibits multiple magnetic transitions below its Néel temperature of 7.6 K. As the holmium ions occupy two different crystallographic positions (2d and 4e) a complex magnetic phase diagram was expected. Former neutron diffraction measurements revealed the existence of at least three different magnetic phases. In order to investigate the phase diagram of the $Ho_3Cu_4Sn_4$ compound in more detail magnetometric, specific heat, transport and high-resolution neutron diffraction measurements were carried out. The specific heat data indicate the occurrence of five magnetic transitions at temperatures of 2.3 K, 3.3 K, 4.4 K, 5.5 K and 7.6 K, which turned out to be in a strict agreement with our new neutron diffraction data. The 2d and 4e rare-earth sublattices order independently at 7.6 K and 3.3 K, respectively. The sublattices are described by different propagation vectors which change with the temperature.

PACS: 65.40.-B; 72.15.Eb; 75.25.+z; 75.30.Cr; 75.30.Kz; 75.30.Sg; 75.50.Ee

Keywords: A. Magnetic intermetallics; B. Electrical resistance and other electrical properties; B. Magnetic properties; F. Calorimetry; F. Diffraction

1. Introduction

The $Ho_3Cu_4Sn_4$ compound belongs to a novel series of rare-earth ternaries $R_3Cu_4X_4$ (R – rare-earth element, X = Si, Ge, Sn) that show interesting physical properties [1]. These compounds crystallize in the orthorhombic $Gd_3Cu_4Ge_4$-type crystal structure (*Immm* space group), in which the rare-earth ions occupy two different crystallographic positions 4e and 2d. Correlations between the two rare-earth sublattices play the key role in the complex magnetic behaviour of these materials. The magnetic, specific heat and neutron diffraction data show that the majority of the $R_3Cu_4X_4$ compounds are antiferromagnetic at low temperatures, and some of them exhibit subsequent magnetic phase transitions in the ordered state [2–10].

The former magnetic and neutron diffraction data collected for $Ho_3Cu_4Sn_4$ indicate the occurrence of at least three phase transitions at 2.5 K, 3.5 K and 8 K [5,6,9], however, neutron diffraction data did not cover all possible magnetic phases. It was suggested that both 4e and 2d magnetic sublattices are ordered up to the Néel point [6]. In order to shed more light on the complex magnetic behaviour of this compound a new sample of a very good quality was made and supplementary magnetic, specific heat, electrical transport and high-resolution neutron diffraction measurements were performed. The results of these studies are reported in the present paper.

2. Experimental

A polycrystalline sample of $Ho_3Cu_4Sn_4$ was obtained by arc melting stoichiometric amounts of the constituent elements

* Corresponding author. Tel.: +48 12 6172904.
E-mail address: lgondek@agh.edu.pl (Ł. Gondek).

0966-9795/$ - see front matter © 2006 Elsevier Ltd. All rights reserved.
doi:10.1016/j.intermet.2006.10.036

(Merck AG: Ho of 99.9% purity, Cu and Sn of 99.99% purity) under high-purity argon atmosphere on a water-cooled copper hearth using titanium–zirconium alloy as a getter. In order to ensure good homogeneity the button was remelted three times. Subsequently the sample was annealed in an evacuated quartz tube at 800 °C for one week. Quality of the product was checked by X-ray powder diffraction at room temperature. The analysis of the X-ray pattern indicated that the sample has the orthorhombic crystal structure of the $Gd_3Cu_4Ge_4$-type with the following lattice parameters: $a = 14.5796(1)$ Å, $b = 6.90736(5)$ Å and $c = 4.41981(3)$ Å. The analysis of the data revealed that the sample is a single phase without impurities.

The magnetic properties were studied in the temperature range 1.7–400 K and in external magnetic fields up to 5 T employing a Quantum Design MPMS-5 SQUID magnetometer. Specific heat measurements were carried out by quasiadiabatic method using a Quantum Design PPMS platform. The bulk sample was prepared in the form of a plate of dimensions 2.5 mm × 2.5 mm × 1 mm. The mass of the sample was 57.1 mg. These measurements were performed in the temperature range of 1.9–300 K and in applied magnetic fields up to 7 T. The electrical resistivity was measured over the 4.2–300 K temperature interval using a standard dc four-probe technique. The current contacts were made using silver paste and the voltage contacts were produced using ultrasonic welding. The Seebeck coefficient was measured from 5 to 300 K using standard differential method with copper as a reference material.

Neutron diffraction experiment was carried out at BERII research reactor (BENSC-HMI) using E9 fine resolution diffractometer. The incident neutron wavelength was 1.79719 Å with a small contamination (5%) of 1.80312 Å, which was taken into account during refinements. The powdered sample of mass of about 8 g was measured in a standard cylindrical vanadium container of diameter 8 mm. Neutron diffraction patterns were collected in the 1.7–11 K temperature range.

3. Results and discussion

3.1. DC magnetic susceptibility

The temperature dependence of the inverse dc magnetic susceptibility is shown in Fig. 1a. Above 10 K the magnetic susceptibility follows the Curie–Weiss law with the paramagnetic Curie temperature $\theta_P = -6.62(6)$ K and the Ho^{3+} effective magnetic moment $\mu_{eff} = 10.03(4)\mu_B$. The sign of θ_P indicates that antiferromagnetic interactions between the rare-earth ions are dominant. The experimental effective magnetic moment is lower than the theoretical free Ho^{3+} ion value of $10.61\mu_B$.

The low-temperature behaviour of the magnetization (Fig. 1b) is quite complex with a broad plateau in between 3.5 and 8 K and a kink at 2.5 K. Moreover, below ca. 6 K little irreversibility is observed in the magnetization curves, taken upon cooling the sample without (ZFC) and in an applied (FC) magnetic field of 0.1 T. The observed features can be attributed to multiple magnetic phase transitions evidenced in the recent neutron diffraction studies [6].

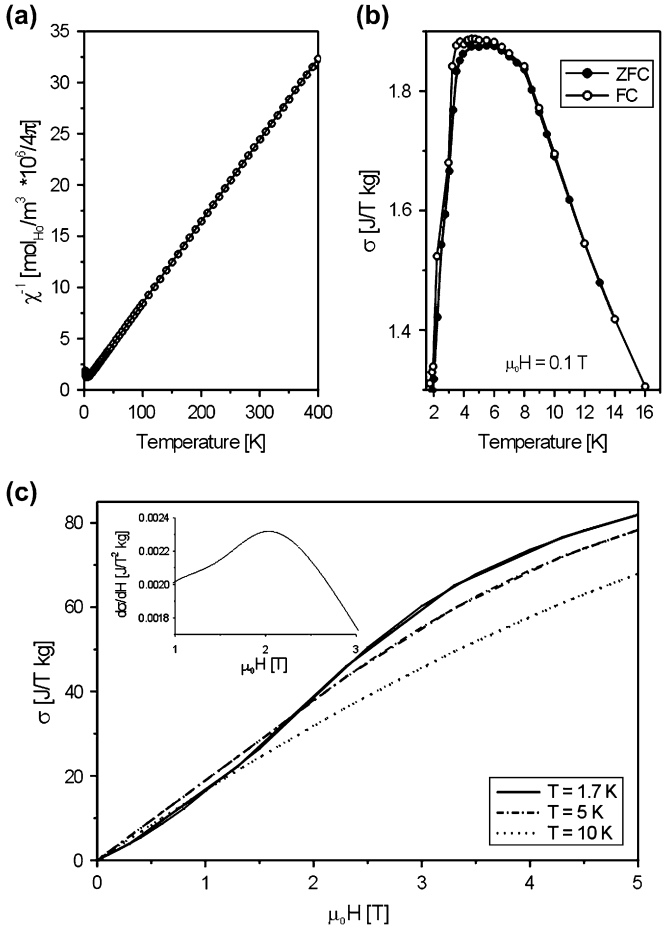

Fig. 1. (a) Temperature dependence of the inverse dc magnetic susceptibility of $Ho_3Cu_4Sn_4$. The solid line is a Curie–Weiss fit. (b) Low-temperature variation of the magnetization. (c) Field dependencies of the magnetization taken at different temperatures. The inset shows derivative dσ/dH at 1.7 K.

In Fig. 1c the magnetization isotherms measured at 1.7 K, 5 K and 10 K are presented. The former curve shows a metamagnetic transition near 2 T, thus proving an essentially antiferromagnetic nature of the ground state (see inset of Fig. 2c). In strong magnetic fields the magnetization tends to saturate, although even at the lowest temperature the saturation is not reached. None of the isotherms exhibits any hysteresis effect when taken with increasing and decreasing magnetic field.

3.2. Specific heat

Fig. 2a displays the specific heat measured in the temperature range of 1.9–300 K in the absence of external magnetic field. The inset shows the low-temperature behaviour. Two sharp λ-type peaks are clearly visible at the temperatures 7.6 K and 3.3 K, whereas additional much weaker anomalies can be noticed at 5.5 K, 4.4 K (very weak) and 2.3 K. All the additional features are visible during heating only (see

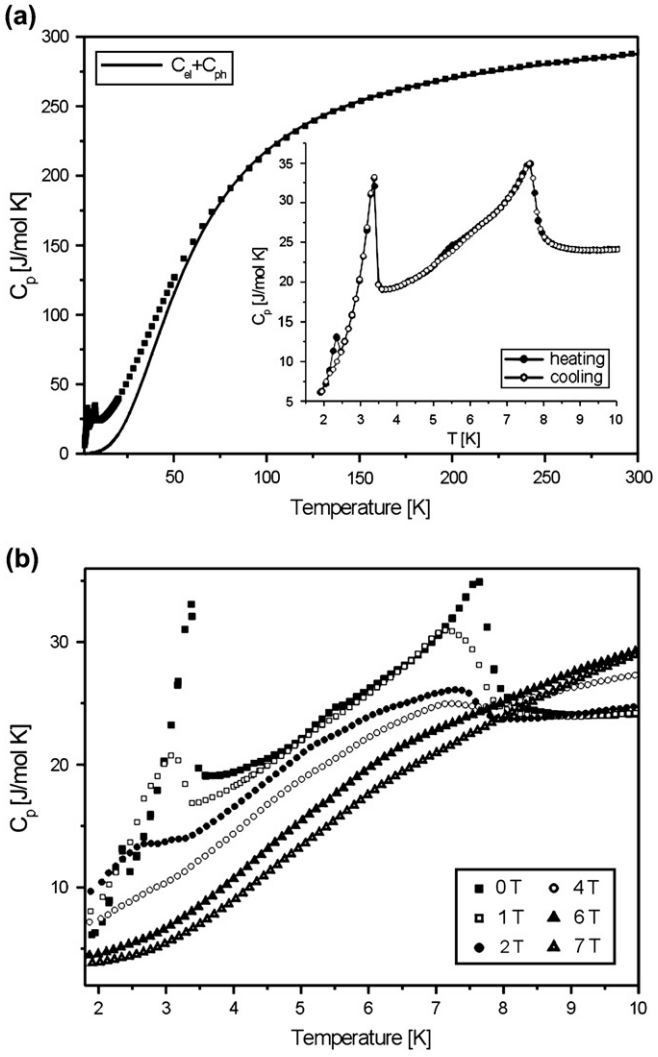

Fig. 2. (a) Temperature dependence of the specific heat of $Ho_3Cu_4Sn_4$ measured in zero-field. The solid line is a fit describing the phonon and electron contributions. The inset blows up the low-temperature region. (b) Low-temperature specific heat measured in applied magnetic field.

the inset of Fig. 2a), thus indicating the first-order transitions. They originate from the magnetic moment reorientations evidenced by neutron diffraction results. A relevant discussion will be given later. The slope change in the onset of the λ peak at 7.6 K may be associated with the transition into an amplitude-modulated phase below that temperature [11]. The jumps of the specific heat at 7.6 K and 3.3 K are only by 11.1 J/mol K and 14.2 J/mol K, respectively, what seem to be a sign of transitions into sine-modulated magnetic structures. Within the mean field model the specific heat jump for Ho-based compound ($J = 8$) should be equal to 20.63 J/mol K in the case of simple (commensurate) magnetic structure, otherwise the jump is expected to be 2/3 of the above value (13.75 J/mol K) [11,12]. As shown in Fig. 2b, upon applying a magnetic field the λ-shaped peaks move towards lower temperatures, as expected for antiferromagnetic transitions. In magnetic fields stronger than 6 T all of the anomalies are totally suppressed.

In order to extract the magnetic part of the specific heat, the lattice and electronic contributions were approximated using the formula:

$$C_{\mathrm{ph+el}} = \frac{9nR}{1-\alpha_{\mathrm{D}}T}\left(\frac{T}{\theta_{\mathrm{D}}}\right)^3 \int_0^{\Theta_{\mathrm{D}}/T} \frac{x^4 \mathrm{e}^x}{\left(\mathrm{e}^x-1\right)^2}\,\mathrm{d}x + \gamma T \qquad (1)$$

where R – gas constant, n – number of ions per formula unit. Fitting Eq. (1) to the experimentally high-temperature specific heat data (note the solid line in Fig. 1a) yielded the Debye temperature $\Theta_{\mathrm{D}} = 230(5)$ K, the Sommerfeld coefficient $\gamma = 15(2)$ mJ/mol K^2 and the anharmonic coefficient $\alpha_{\mathrm{D}} = 2.1(3) \times 10^{-4}$ K^{-1}. So-derived reference curve is in an agreement with data of Y-based analogue presented in Ref. [2]. The anharmonic correction was considered because the specific heat values at room temperature exceeded the Dulong–Petit limit $3nR = 274.23$ J/mol K.

Assuming that the nonmagnetic contributions to the specific heat remain unperturbed in an external magnetic field, the variations of the Schottky contribution to the measured specific heat in fields up to 7 T were estimated. Fig. 3 shows the magnetic specific heat derived from the data collected in zero-field and in the field of 7 T. As holmium ions in $Ho_3Cu_4Sn_4$ occupy two different crystallographic positions the total Schottky effect should be attributed to two terms with the weights corresponding to the multiplicity of the appropriate atomic sites:

$$C_{\mathrm{Schottky}} = 2\frac{R}{T^2}\left[\frac{\sum_{i=1}^{17} E_i^2 \mathrm{e}^{-E_i/T}}{\sum_{i=1}^{17} \mathrm{e}^{-E_i/T}} - \left(\frac{\sum_{i=1}^{17} E_i \mathrm{e}^{-E_i/T}}{\sum_{i=1}^{17} \mathrm{e}^{-E_i/T}}\right)^2\right]$$

$$+\frac{R}{T^2}\left[\frac{\sum_{i=1}^{17} W_i^2 \mathrm{e}^{-W_i/T}}{\sum_{i=1}^{17} \mathrm{e}^{-W_i/T}} - \left(\frac{\sum_{i=1}^{17} W_i \mathrm{e}^{-W_i/T}}{\sum_{i=1}^{17} \mathrm{e}^{-W_i/T}}\right)^2\right] \qquad (2)$$

where E_i and W_i denote the energies (in Kelvin) of crystal field (CF) levels at the 4e and 2d positions, respectively. Due to point symmetries of both positions (C_{2v} and D_{2h} for 4e and 2d sites, respectively) the set of nine parameters of CF Hamiltonian must be taken into account: B_2^0, B_2^2, B_4^0, B_4^2, B_4^4, B_6^0, B_6^2, B_6^4, B_6^6. In such a case, the $^5I_8$ ground multiplet of non-Kramers Ho ion splits into $(2J+1)$ singlets. As one can realize there are more than 30 free parameters to fit formula (2) to the experimental data, which make any refinement quite ambiguous. However, some general remarks can be made. The direct fit of formula (2) to the data collected in zero magnetic field (the regions of the λ peaks were excluded) is shown in Fig. 3 as the solid line. The conclusions are as follows:

- the lowest lying CF states (E_1 and W_1) are singlets for both atomic positions. This is reasonable as holmium is a non-Krammers' ion,

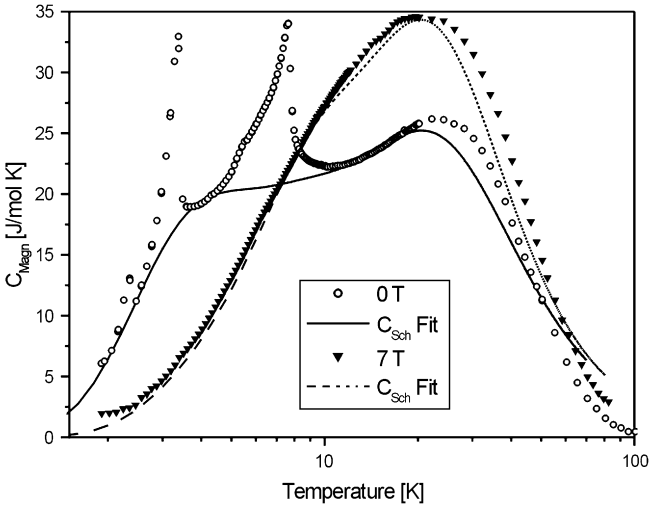

Fig. 3. Temperature variation of the magnetic contribution to the specific heat of $Ho_3Cu_4Sn_4$ in external magnetic fields of 0 and 7 T. The lines denote the calculated Schottky contributions (see text for detail).

- the first excited levels (E_2 and W_2) are located at about 8 K above the E_1 and W_1 levels,
- the overall splittings of the ground multiplets do not exceed 100 K.

Similarly, fit of formula (2) to the data taken in the magnetic field of 7 T (note the dashed line in Fig. 3) leads to following conclusions:

- the CF ground states E_1 and W_1 are singlets,
- the energy gap between E_2 and E_1 rises to 14 K and that between W_2 and W_1 increases to 30 K,
- the overall splitting of the CF levels for both atomic sites is close to 100 K.

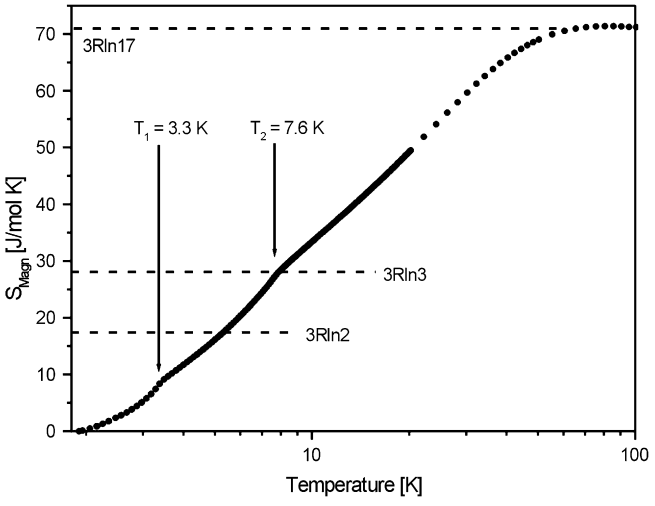

Fig. 4. Temperature dependence of the magnetic entropy in $Ho_3Cu_4Sn_4$ without external magnetic field. Positions of the main λ peaks are marked with arrows.

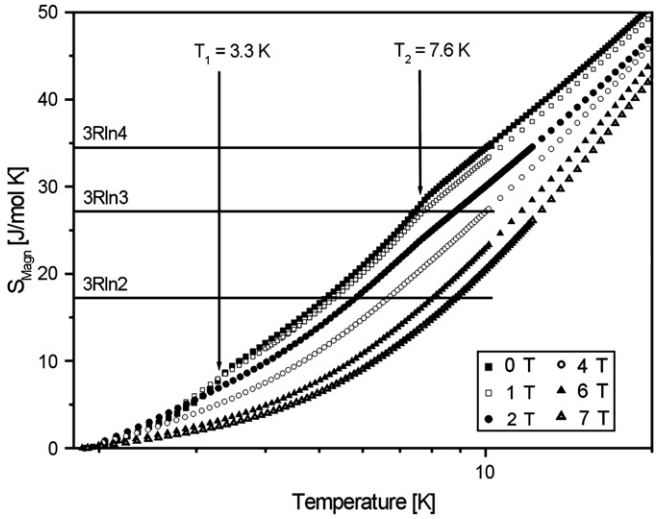

Fig. 5. Temperature variations of the magnetic entropy in $Ho_3Cu_4Sn_4$ in external magnetic fields. Positions of the λ peaks are marked with arrows.

3.3. Magnetic entropy and magnetocaloric effect

From the evaluated magnetic contribution to the specific heat the magnetic entropy can be calculated according to the formula $S_{\mathrm{Magn}}(T) = \int_0^T (C_{\mathrm{Magn}}(T')/T')\,\mathrm{d}T'$. Fig. 4 displays the results obtained from the zero-field data. Apparently, at

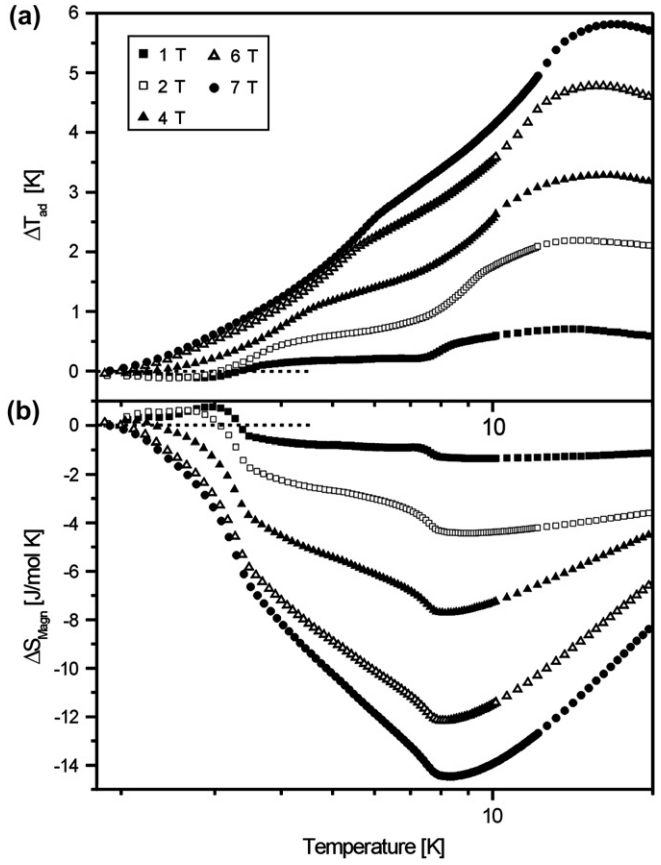

Fig. 6. (a) Adiabatic temperature change and (b) magnetic entropy change versus temperature for $Ho_3Cu_4Sn_4$ in external magnetic fields up to 7 T.

Table 1
Characteristic temperatures of the magnetocaloric effect (all data in Kelvin)

$H_{ext}\downarrow$	Θ_1	Θ_2	Θ_3	Θ_4	Θ_5	Θ_6
	T_1/S_1	T_2/S_2	T_3/S_3	T_4/S_4	T_5/S_5	T_6/S_6
1 T	2.2 –/2.2	2.4 –/2.4*	2.9 2.8*/2.9	6.6 6.4/6.4*	7.1 7.2*/7.1	9.4 13.5/9.4*
2 T	–	–	2.6 2.4*/2.6	–	–	8.9 14.1/9.0*
4 T	–	–	–	–	–	8.1 16.2/8.0*
6 T	–	–	–	–	–	8.1 15.7/8.1*
7 T	–	–	–	–	–	8.3 16.5/8.2*

Upper rows: Θ_i points where $C_P(0,T) = C_P(H,T)$. Lower rows: T_i and S_i points derived from the $\Delta T_{ad}(T)$ and $\Delta S_{Magn}(T)$ curves, respectively (minima are marked by the '*' symbol).

100 K the entire $^5I_8$ multiplets of Ho^{3+} ions are populated, consequently the observed magnitude of S_{Magn} is close to the value of $3R \ln 17$ expected for the Schottky contribution. The magnetic phase transitions at 3.3 K and 7.6 K manifest themselves as distinct kinks on the temperature variation of the entropy. The entropy values at these temperatures correspond well with the above conclusions of the analysis of the Schottky effect. The magnetic entropy variations calculated from the specific heat data taken in magnetic fields up to 7 T are shown in Fig. 5. Clearly, no kinks due to magnetic transitions are visible in fields stronger than 4 T.

The magnetocaloric effect (MCE) can be investigated by calculating the adiabatic temperature change ΔT_{ad} (Fig. 6a) and the isothermal magnetic entropy change ΔS_{Magn} (Fig. 6b) using the standard approach described in Refs. [13,14]. The change of the sign of both MCE curves near 3 K is probably due to the first-order phase transition observed at 2.3 K [15].

Some characteristic points Θ_i of crossings of the specific heat curves $C_P(T)$ measured in zero and non-zero magnetic fields can be related to minima or maxima on the MCE curves [16]. When considering the 0 and 1 T specific data of $Ho_3Cu_4Sn_4$, one can discriminate the following points Θ_i (see Fig. 2b): Θ_1 and Θ_2 are due to the first-order transition at 2.3 K, Θ_3 and Θ_6 are associated with the λ peaks at 3.3 K and 7.6 K, respectively, as well as Θ_4 and Θ_5 which are related to a weak structure in the onset of the λ peak in the vicinity of 6 K. In the case of the 0 and 2 T data only the Θ_3 and Θ_6 points can be identified, while for stronger fields a single Θ_6 point persists. Table 1 gives a comparison of the so-derived Θ_i temperatures with the positions of the extremes in the ΔT_{ad} and ΔS_{Magn} curves (denoted as T_i and S_i, respectively). Apparently, there is a good agreement between the characteristic temperatures, especially with those of Θ_i and S_i points. The only exception is a maximum T_6 occurring in $\Delta T_{ad}(T)$

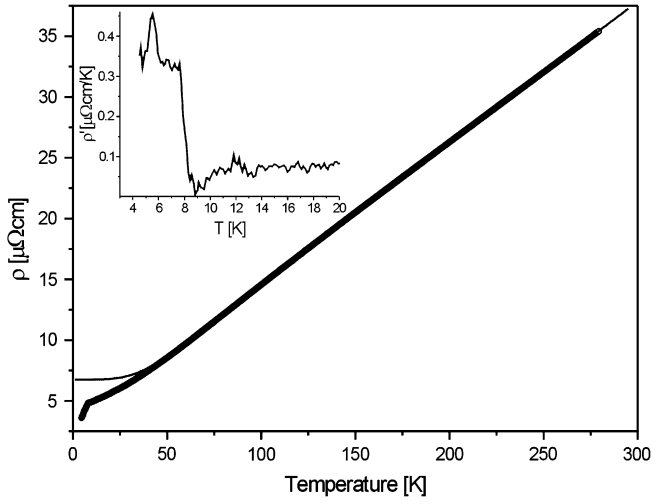

Fig. 7. Temperature dependence of the electrical resistivity of $Ho_3Cu_4Sn_4$. The solid line represents the fit discussed in the text. The inset shows the first temperature derivative of $\rho(T)$.

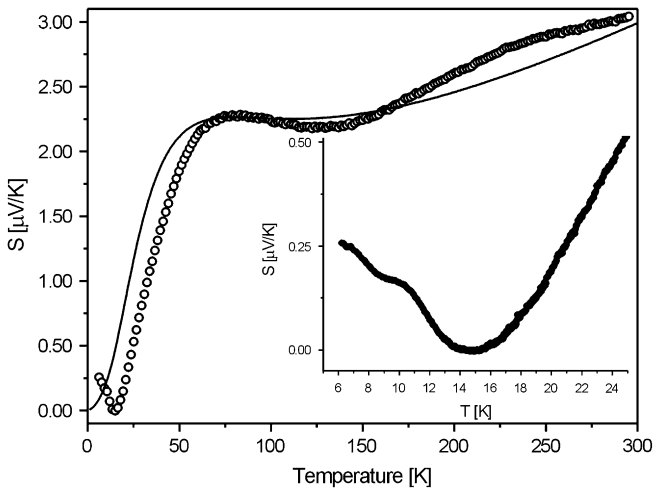

Fig. 8. Temperature variation of the Seebeck coefficient of $Ho_3Cu_4Sn_4$. The solid line is the fit discussed in the text. The inset zooms in the low-temperature region.

Table 2
Structural parameters of $Ho_3Cu_4Sn_4$ at low temperatures derived from neutron diffraction data

T (K)	a (Å)	b (Å)	c (Å)	V (Å^3)	x_{Ho}	x_{Cu}	x_{Sn}	R_{Bragg} (%)
						y_{Cu}	y_{Sn}	R_F (%)
1.7	14.5387(10)	6.8842(4)	4.4074(2)	441.12(4)	0.1299(8)	0.3265(6)	0.2173(10)	6.3
						0.1863(12)	0.2000(16)	3.9
3	14.5394(10)	6.8851(4)	4.4074(2)	441.21(4)	0.1301(8)	0.3265(6)	0.2162(10)	6.6
						0.1862(12)	0.2001(16)	4.1
4	14.5381(10)	6.8842(4)	4.4072(2)	441.09(4)	0.1295(8)	0.3264(6)	0.2172(10)	7.1
						0.1863(12)	0.1998(18)	4.7
5	14.5380(8)	6.8842(4)	4.4071(2)	441.07(4)	0.1294(8)	0.3263(6)	0.2171(8)	7.3
						0.1860(12)	0.2002(18)	4.8
6	14.5383(8)	6.8837(4)	4.4068(2)	441.02(4)	0.1296(8)	0.3264(6)	0.2175(8)	7.1
						0.1859(12)	0.2012(18)	4.9
7	14.5382(8)	6.8833(4)	4.4067(2)	440.99(4)	0.1295(8)	0.3264(6)	0.2175(8)	5.7
						0.1860(12)	0.2011(18)	4.2
11	14.5384(10)	6.8834(4)	4.4071(2)	441.03(4)	0.1312(10)	0.3269(8)	0.2174(10)	8.9
						0.1877(10)	0.1987(18)	6.2

Standard deviations are given in parentheses. The reliability factors are listed in the last column.

at about 15 K, which does not correlate with the point Θ_6 derived from the specific heat data.

3.4. Electrical resistivity

The temperature dependence of the electrical resistivity is presented in Fig. 7. At room temperature the resistivity is about 35 μΩ cm. With decreasing temperature it diminishes in a metallic manner reaching about 5 μΩ cm just above the onset of the long-range magnetic order setting at 7.8 K. The magnetic phase transition manifests itself as a pronounced kink on the $\rho(T)$ curve that results in a jump in the derivative $d\rho/dT$ (see the inset in Fig. 7). Another sharp anomaly in $d\rho/dT(T)$ occurs at 5.5 K, i.e. at the characteristic temperature identified in both the magnetization and the specific heat studies. Unfortunately no evidence for the other phase transitions at lower temperatures could be obtained because in the performed resistivity measurements the temperature was limited to 4.2 K.

In the paramagnetic region the electrical resistivity was analysed in terms of the Bloch–Grüneisen–Mott formula [17]:

$$\rho(T)=\left(\rho_0+\rho_0^{\infty}\right)+4RT\left(\frac{T}{\Theta_D}\right)^4\int_0^{\Theta_D/T}\frac{x^5\,dx}{(e^x-1)(1-e^{-x})}-KT^3 \quad (3)$$

which describes scattering conduction electrons on static defects in the crystal lattice (the residual resistivity ρ_0), disordered magnetic moments (the spin-disorder resistivity ρ_0^{∞}), and phonons (second term). The third term accounts for s–d interband scattering processes. Fitting Eq. (3) to the resistivity data above 50 K yielded the following values of the parameters: $\rho_0+\rho_0^{\infty} = 6.7(2)$ μΩ cm, $\Theta_D = 234(4)$ K, $R = 0.104(5)$ μΩ cm/K and $K = 3.81(1)\times10^{-8}$ μΩ cm/K^3. Worth noting is that the so-derived Debye temperature Θ_D is almost equal to that determined from the specific heat, which implies relatively weak electron–electron correlations [18]. The value of K is very small, thus indicating a nearly negligible contribution from Mott-type processes, as may also be concluded from approximately linear behaviour of $\rho(T)$ at high temperatures. The sum of $\rho_0+\rho_0^{\infty}$ contains a contribution from spin-disorder scattering that is temperature independent only in the region where crystal field effects can be neglected. For $Ho_3Cu_4Sn_4$ such an assumption seems valid for the electrical transport phenomena roughly above 50 K. At lower temperatures a more and more significant deviation of the experimental data from the calculated resistivity curve is observed because of a gradual depopulation of excited crystal field levels with decreasing temperature.

3.5. Thermoelectric power

The temperature variation of the Seebeck coefficient $S(T)$ is shown in Fig. 8. The positive sign of the thermopower in the entire temperature range suggests that the major role in the electrical transport is probably played by the holes [19]. At low temperatures $S(T)$ exhibits a tiny anomaly occurring at the Néel point (see the inset of Fig. 8). In the paramagnetic region the thermopower shows strongly non-linear temperature dependence with a deep minimum at 14.7 K and a broad bump near 70 K. The latter anomaly may be interpreted as being caused by the so-called phonon-drag effect [20] that results in the formation of a maximum in $S(T)$ at a temperature of $0.1-0.3\Theta_D$ [21]. For $Ho_3Cu_4Sn_4$ the Debye temperature Θ_D estimated from the specific heat and resistivity data is about 230 K, thus this mechanism seems to be quite a likely one.

Another quantitative explanation of the non-linear behaviour of $S(T)$ is provided by models that consider perturbations of nearly free electron gas via inelastic scattering on phonons and/or impurities [22,23]. In the frame of the inelastic

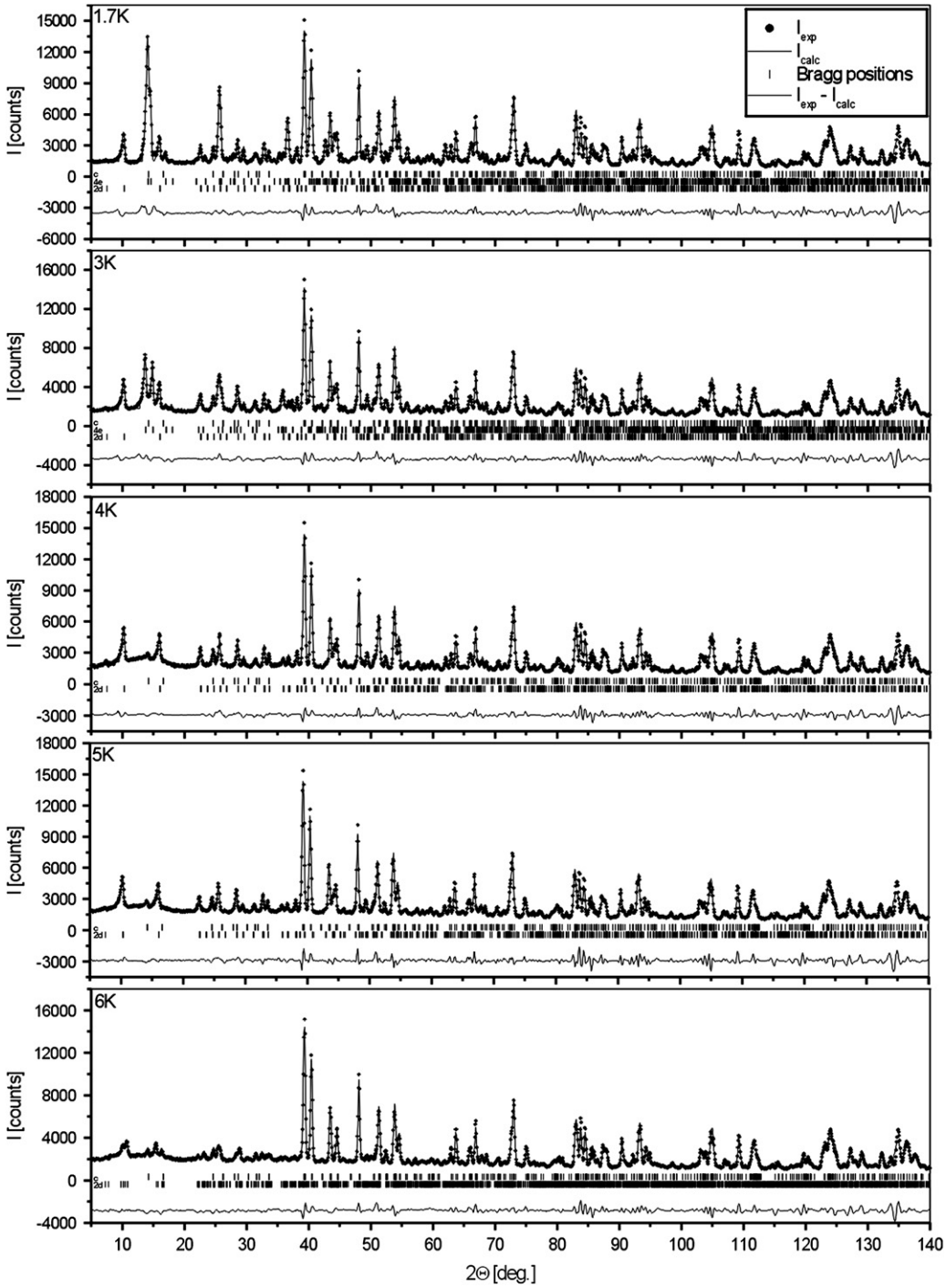

Fig. 9. Neutron diffraction patterns of $Ho_3Cu_4Sn_4$ recorded in different magnetic phases below the Néel temperature. Bragg positions originating from crystal structure are labelled as c, whereas positions originating from magnetically ordered phases are labelled by 2d and 4e with respect to the 2d and 4e rare-earth sublattices, respectively.

electron–phonon scattering model developed in Refs. [19,24] the thermoelectric power can be expressed by the function:

$$S(T) = S_0(t) + (t/c)S_1(t) \tag{4}$$

where $t = T/\Theta_D$, $c = \varepsilon_F/k_B\Theta_D$ (ε_F – Fermi energy) and the functions $S_i(t)$ are given by:

$$S_0(t) = \frac{\pi^2}{3}\frac{k_B}{e}\frac{P_{12}(t)}{P_{22}(t)} \tag{5a}$$

$$S_1(t) = -\frac{\pi^2}{3}\frac{k_B}{e}\left[1 + \frac{\pi^3}{3}\frac{P_{11}(t)}{P_{22}(t)}\right] \tag{5b}$$

with $P_{ij}(t)$ being the scattering matrix elements dependent on the parameter $\varepsilon_S = 2m_e v_s^2$, where m_e stands for the electron mass and v_s is the sound velocity (for detailed definitions see Ref. [24]).

Upon modifying Eqs. (4) and (5a) to the form valid for holes and introducing a scaling factor α

$$S(T) = \alpha\left(\tilde{S}_0(t) - \frac{t}{c}S_1(t)\right) \tag{6}$$

the model was fitted to the experimental data of $Ho_3Cu_4Sn_4$ measured above 20 K. The resulting fit is marked in Fig. 8 by the solid line, and the so-derived parameters are as follows: $\varepsilon_F = 3100(17)$ K, $\varepsilon_S = 4.5(3)$ K and $\Theta_D = 195(9)$ K. The Debye temperature is in a rather good agreement with the other estimates from the specific heat and the resistivity data (see above), especially if one takes into account the simplicity of the applied model.

Finally, it is worthwhile mentioning that a behaviour somewhat similar to that shown in Fig. 8 is frequently observed for so-called heavy-fermion compounds and interpreted in the framework of the Hirst model [25,26]. However, the latter approach assumes the presence of a narrow f-electron band in the vicinity of the Fermi level. This scenario seems quite unlikely for $Ho_3Cu_4Sn_4$ that unambiguously is a stable moment system.

3.6. Neutron diffraction

3.6.1. Crystal structure

Neutron diffraction measurements confirmed that in low temperatures (down to 1.7 K) the compound crystallizes in the orthorhombic *Immm* structure. In this structure the Ho atoms occupy two different crystallographic positions 2d (0.5, 0, 0.5) and 4e (x_{Ho}, 0, 0), the Cu atoms are placed at the 8n (x_{Cu}, y_{Cu}, 0) position and the Sn atoms occupy the 4f (x_{Sn}, 0.5, 0) and the 4h (0, y_{Sn}, 0.5) positions. All structural parameters are listed in Table 2. According to the analysis of all collected patterns no changes in crystal structure, accompanying consequent magnetic transitions, were observed. The refinements of the data were made using Rietveld-type FullProf software [27].

3.6.2. Magnetic structure

Neutron diffraction patterns were recorded at seven temperatures in order to describe all possible magnetic phases suggested by specific heat measurements. It turned out that all five magnetic phases suggested by specific heat measurements were observed. In Fig. 9 five patterns collected at 1.7 K, 3 K, 4 K, 5 K and 6 K in different magnetic phases are presented. Fig. 10 shows low-angle part of neutron diffraction patterns presented in Fig. 9. The complete refinement results including magnetic structure as well as respective reliability factors are tabulated in Table 3. The magnetic structures described by incommensurate propagation vectors are considered as

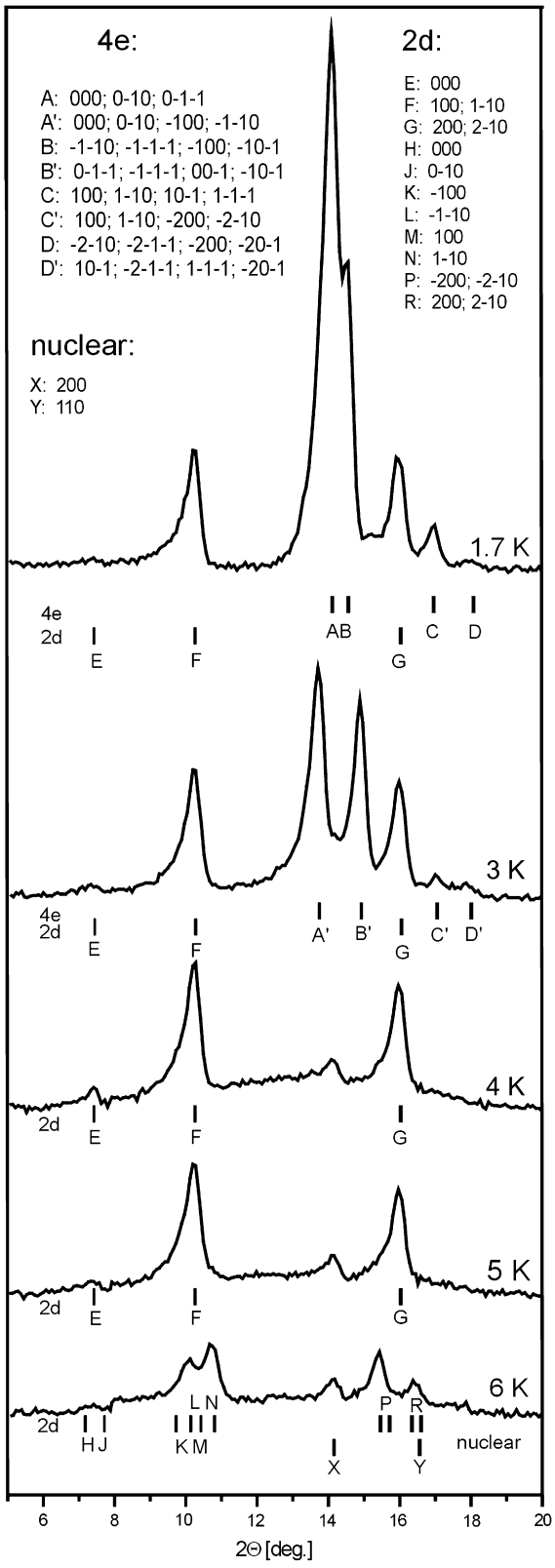

Fig. 10. Low-angle part of neutron diffraction patterns taken in the magnetically ordered state. Groups of reflections are labelled with respect to both magnetic sublattices 4e and 2d. Nuclear reflections are given only in bottom diagram. Each reflection is denoted with capital latter, to which an appropriate index is attributed in the upper part of the picture.

Table 3
Magnetic ordering of $Ho_3Cu_4Sn_4$

T (K)	μ_{2d} (μ_B)	2d: θ (°) and φ (°)	k_{2d}	$R_{F(2d)}$ (%)
	μ_{4e} (μ_B)	4e: θ (°) and φ (°)	k_{4e}	$R_{F(4e)}$ (%)
1.7	8.3(2)	90 and 90	0;0.5;0	9.8
	9.9(2)	90 and 0	0.3712(14);0.5;0.5	7.9
3	8.6(2)	90 and 90	0;0.5;0	10.0
	8.0(2)	90 and 0	0.5;0.5;0.4694(2)	9.9
4	8.6(2)	80(2) and 90	0;0.5;0	12.2
	–	–	–	–
5	8.5(2)	90 and 90	0;0.5;0	12.9
	–	–	–	–
6	9.1(2)	90 and 77(4)	0.0695(18);0.4821(16);0	15.3
	–	–	–	–
7	9.0(2)	90 and 76(4)	0.067(2);0.480(2);0	15.9
	–	–	–	–

μ_{2d} and μ_{4e} – denotes Ho magnetic moments in 2d and 4e sublattices. Parameters θ and φ denote angles that are formed between magnetic moments and the c-axis and a-axis, respectively. k_{2d} and k_{4e} are propagations vectors for 2d and 4e sublattice, respectively. Standard deviations are given in parentheses. The reliability factors are listed in the last column.

amplitude modulated. Within the crystal unit cell magnetic Ho ions occupy following positions:

$$\mathrm{M1}(x_{Ho};\,0;\,0),\ \mathrm{M2}(1-x_{Ho};\,0;\,0),\ \mathrm{M3}(\tfrac{1}{2}+x_{Ho};\,\tfrac{1}{2};\,\tfrac{1}{2}),$$
$$\mathrm{M4}(\tfrac{1}{2}-x_{Ho};\,\tfrac{1}{2};\,\tfrac{1}{2}) - \text{for the 4e sublattice}$$

$$\mathrm{M5}(\tfrac{1}{2};\,0;\,\tfrac{1}{2}),\ \mathrm{M6}(0;\,\tfrac{1}{2};\,0) - \text{for the 2d sublattice}$$

where x_{Ho} changes with the temperature (see Table 2 for details).

At 1.7 K both 2d and 4e magnetic sublattices are ordered. The magnetic moments of 2d sublattice are parallel to the b-axis, whereas the ones of 4e sublattice are parallel to the a-axis. The magnetic structure was found to be very close to that reported earlier [6], with propagation vectors $k_{4e} = (0.3712(14);0.5;0.5)$ and $k_{2d} = (0;0.5;0)$ for 4e and 2d sublattices, respectively. Within the crystal unit cell the sequences of magnetic moments are $[++--]$ for 4e and $[++]$ for the 2d sublattice. The sequence of magnetic moments of 2d sublattice does not change up to the Néel temperature.

The analysis of pattern recorded at 3 K reveals a change of propagation vector in 4e sublattice. Now $k_{4e} = (0.5;0.5;0.4694(2))$, however, magnetic moments are still parallel to the a-axis. They are ordered in $[++++]$ sequence. This change is reflected with splitting of reflections A and B (see Fig. 10). The ordering of the 2d sublattice remains unchanged.

In contrast to Ref. [6] above 3.3 K the 4e sublattice is no longer ordered. This is consistent with the specific heat measurements reported in Section 3.2. At 4 K the propagation vector k_{2d} describing the 2d sublattice is still commensurate (0;0.5;0), however, the orientation of magnetic moment is slightly changed. Now the magnetic moments lie in the b–c plane and form an angle of 10(2)° with the b-axis. The above-mentioned reorientation can be recognized as an intensity increase of E magnetic reflection at about 7.5° of 2Θ angle (see Fig. 10). Within 5°–20° range of 2Θ angle a diffusive scattering resulting with a very broad bump in background is visible. This effect is related to some short-range correlations within disordered 4e sublattice.

A closer inspection of pattern collected at 5 K reveals vanishing of E reflection, which is a sign that 2d magnetic moments lie along the b-axis again. This reorientation is hardly visible in specific heat data as a small irreversibility at 4.4 K with respect to cooling and heating curves (see inset of Fig. 2a).

At 6 K a change of propagation vector from commensurate into incommensurate one is visible. Splitting of F and G reflections can be noticed, which is presented in Fig. 10. The new propagation vector is $k_{2d} = (0.0695(18);0.4821(16);0)$. The magnetic structure is changed a little in comparison to 5 K structure. The magnetic moments lie in the a–b plane forming an angle of 23(4)° with the b-axis. The pattern collected at 7 K does not exhibit any significant changes of magnetic ordering (see Table 3). The existence of non-collinear magnetic structure just below T_N was observed in many rare-earth intermetallic compounds and was explained theoretically [28].

At 11 K magnetic moments of Ho do not exhibit long-range order.

The above results show that magnetic moments in both sublattices are parallel to each other. It may be caused by the Dzialoshinsky–Moriya interactions as well as by the crystal electric field effects. The latter seem to be more probable as the different point symmetries of 2d and 4e positions may be responsible of different preferable direction of magnetic moments in each sublattice. The independent ordering of both sites leads to a conclusion that coupling between 2d and 4e magnetic moments must be relatively weak. One may speculate that oscillatory character of RKKY interactions may lead to diminishing of the exchange integrals between both sublattices.

4. Summary

The results presented above show complex nature of the magnetism in antiferomagnetically ordered $Ho_3Cu_4Sn_4$. Specific heat and transport measurements revealed that the Debye temperature is about 220 K. Sample exhibits metallic behaviour with relatively weak electron correlations, however, a strongly non-linear dependence of thermoelectric power at temperatures close to the Debye temperature implies some electron–electron correlations to be present. As the shortest distance between rare-earth ions is close to 4 Å the indirect RKKY model is believed to be responsible of magnetic ordering.

Based on the new neutron diffraction results presented above it was possible to find five different magnetic phases below the Néel temperature, which is in a strict agreement with specific heat studies. The two distinct λ peaks visible in the specific heat at 7.6 K and 3.3 K are unambiguously due to independent ordering of holmium magnetic moments at 2d and

4e sites, respectively. A similar behaviour was observed in large number of 3:4:4 compounds [29].

Acknowledgements

This research project has been supported by the European Commission under the 6th framework programme through the Key Action: Strengthening the European Research Area, Research Infrastructures. Contract no.: RII3-CT-2003-505925 (NMI3).

The authors are grateful to Dr. D. Badurski and Dr. K. Gofryk for their assistance in electrical resistivity and thermoelectric power measurements, respectively.

One of us (ŁG) would like to express gratitude to the BENCS Management for their kind hospitality.

References

[1] Thirion F, Steinmetz J, Malaman B. Mater Res Bull 1983;18:1537.
[2] Singh S, Dhar SK, Manfrinetti P, Palenzona A. J Alloys Compd 2000;298:68.
[3] Singh S, Dhar SK, Manfrinetti P, Palenzona A. J Magn Magn Mater 2002;250:190.
[4] Zaharko O, Keller L, Ritter C. J Magn Magn Mater 2002;253:130.
[5] Szytuła A, Wawrzyńska E, Penc B, Stüsser N, Zygmunt A. Physica B 2003;327:167.
[6] Wawrzyńska E, Hernandez-Velasco J, Penc B, Sikora W, Szytuła A, Zygmunt A. J Phys Condens Matter 2003;15:5279.
[7] Wawrzyńska E, Hernandez-Velasco J, Penc B, Szytuła A. J Phys Condens Matter 2004;16:45.
[8] Szytuła A, Wawrzyńska E, Penc B, Hernandez-Velasco J, Zygmunt A. J Magn Magn Mater 2004;272–276:618.
[9] Wawrzyńska E, Hernandez-Velasco J, Penc B, Szytuła A. Physica B 2004;350:e127.
[10] Ryan DH, Cadogan JM, Gagnon R, Swainson IP. J Phys Condens Matter 2004;16:3183.
[11] Blanco JA, Gignoux D, Schmitt D. Phys Rev B 1991;43:13145.
[12] Sereni JG. Specific heat. In: Buschow KHJ, Gratz E, editors. Encyclopedia of materials: science and technology. Oxford: Elsevier Science Ltd; 2001.
[13] Pecharsky VK, Gschneidner KA. J Appl Phys 1999;86:565.
[14] Pecharsky VK, Gschneidner KA, Pecharsky AO, Tishin AM. Phys Rev B 2001;64. 144406.
[15] Tegus O, Brück E, Zhang L, Dagula, Buschow HJK, de Boer FR. Physica B 2002;319:174.
[16] Tishin AM, Gschneidner KA, Pecharsky VK. Phys Rev B 1999;59:503.
[17] Mott NF, Jones H. The theory of the properties of metals and alloys. Oxford: Oxford University Press; 1958.
[18] Giovannini M, Michor H, Bauer E, Hilscher G, Rogl P, Ferro R. J Alloys Compd 1998;280:26.
[19] Durczewski K, Ausloos M. Phys Rev B 1994;49:13215.
[20] Ziman JM. Electrons and phonons. Oxford: Oxford University Press; 1967.
[21] Blatt F, Schroeder P, Foiles C, Greig D. Thermoelectric power of metals. New York: Plenum; 1976.
[22] Nielsen PE, Taylor PL. Phys Rev B 1974;10:4061.
[23] Nielsen PE, Taylor PL. Phys Rev Lett 1970;25:371.
[24] Durczewski K, Ausloos M. Phys Rev B 2000;5303.
[25] Gottwick U, Gloos K, Horn S, Steglich F, Grewe N. J Magn Magn Mater 1985;47–48:536.
[26] Park J-G, Očko M. J Phys Condens Matter 1997;9:4627.
[27] Rodriguez-Carvajal J. Physica B 1993;192:55.
[28] Gignoux D, Schmitt D. Phys Rev B 1993;48:12682.
[29] Wawrzyńska E. Thesis. Kraków: Jagiellonian University; 2005.